

# Emergent quantum disordered phase in $\text{Na}_2\text{Co}_2\text{TeO}_6$ under intermediate magnetic field along $c$ axis

Xu-Guang Zhou,<sup>1,\*</sup> Han Li,<sup>2,3,\*</sup> Chaebin Kim,<sup>4,5,\*</sup> Akira Matsuo,<sup>1</sup> Kavita Mehlawat,<sup>1</sup>

Kazuki Matsui,<sup>1</sup> Zhuo Yang,<sup>1</sup> Atsuhiko Miyata,<sup>1</sup> Gang Su,<sup>2</sup> Koichi Kindo,<sup>1</sup>

Je-Geun Park,<sup>4,6</sup> Yoshimitsu Kohama,<sup>1,†</sup> Wei Li,<sup>3,‡</sup> and Yasuhiro H. Matsuda<sup>1,§</sup>

<sup>1</sup>*Institute for Solid State Physics, University of Tokyo, Kashiwa, Chiba 277-8581, Japan*

<sup>2</sup>*Kavli Institute for Theoretical Sciences, University of Chinese Academy of Sciences, Beijing 100190, China*

<sup>3</sup>*CAS Key Laboratory of Theoretical Physics, Institute of Theoretical Physics, Chinese Academy of Sciences, Beijing 100190, China*

<sup>4</sup>*Center for Quantum Materials, Seoul National University, Seoul 08826, Republic of Korea*

<sup>5</sup>*School of Physics, Georgia Institute of Technology, Atlanta, Georgia 30332, USA*

<sup>6</sup>*Department of Physics and Astronomy, Institute of Applied Physics, Seoul National University, Seoul 08826, Republic of Korea*

Identifying the exotic quantum spin liquid phase in Kitaev magnets has garnered great research interests and remains a significant challenge. In experiments, most of the proposed candidate materials exhibit an antiferromagnetic (AFM) order at low temperatures, thus the challenge transforms into the searching for a field-driven disordered phase that is distinct from the partially polarized paramagnetic phase after suppressing the AFM order. Recently,  $\text{Na}_2\text{Co}_2\text{TeO}_6$  has been proposed as one of the prime candidates, where the Kitaev interaction is realized by the high-spin  $t_{2g}^5 e_g^2$  configuration, and spin-orbit entangled  $J_{\text{eff}} = 1/2$  state in a bond-edge shared honeycomb lattice. In this study, we identify an emergent intermediate disordered phase induced by an external field along the  $c$ -axis of the honeycomb plane. This phase is characterized through magnetization and magnetocaloric effect experiments in high magnetic fields. To explain the experimental results, we propose an effective spin model with large AFM Kitaev interaction, which yields results in good agreement with both our findings and previously reported data. We determine that the effective  $K$ - $J$ - $\Gamma$ - $\Gamma'$  model for  $\text{Na}_2\text{Co}_2\text{TeO}_6$  is nearly dual to that of  $\alpha$ - $\text{RuCl}_3$  under an unitary transformation. Given the insignificant fragility of  $\text{Na}_2\text{Co}_2\text{TeO}_6$  sample, further high-field experiments can be conducted to explore this intermediate-field quantum spin disordered phase.

## I. INTRODUCTION

The spin-1/2 Kitaev honeycomb model with bond-dependent nearest-neighbor Ising-type exchange interactions is notable for being exactly solvable two dimensions system and hosting a quantum spin liquid (QSL) ground state [1]. As a quantum disordered spin state, it exhibits long-range quantum entanglement and fractionalized excitations, making it promising platform for topological quantum computation [2, 3]. Over the past decade, experimental efforts have focused on realizing the Kitaev model in honeycomb layered compounds with  $4d$  and  $5d$  transition-metal ions [4–6]. These studies highlight that Heisenberg interactions ( $J$ ) and off-diagonal terms ( $\Gamma$ ) must also be considered, leading to ordered ground states [7–9]. Nevertheless, Kitaev physics could still be realized in proximate Kitaev materials when the Kitaev term ( $K$ ) is dominant.

Among the heavy transition metal candidates,  $\alpha$ - $\text{RuCl}_3$  stands out as a promising material [10–12]. Despite its ground state being a zigzag antiferromagnetic (AFM) ordered state, several strong experimental evi-

dences suggest the emergence of the QSL phase under in-plane magnetic fields with the suppression of the zigzag spin order [9, 13, 14]. These evidences include the continuum excitation observed by inelastic neutrons, quantized thermal Hall conductivity, and the possible switching of the Majorana excitation gap [9, 13–16]. Nonetheless, this in-plane field-induced intermediate phase in  $\alpha$ - $\text{RuCl}_3$  lacks support from thermodynamic experimental results and theoretical calculations [7, 17] based on its microscopic spin models [18–20].

In contrast, under an out-of-plane field, an intermediate-field phase is proposed by both ground-state and finite-temperature calculations for the effective  $\alpha$ - $\text{RuCl}_3$  model, which is further confirmed by the angle-field phase diagram from magnetization measurements up to 100 T [20–22]. Such intermediate-field phase is considered a QSL confirmed in both the thermal and ground-state calculations [20, 21]. Although the magnetization and torque experiments have been reported in high out-of-plane magnetic field, the large magnetic torque and fragility of  $\alpha$ - $\text{RuCl}_3$  prevent to perform further investigations of the possible QSL phase experimentally [21, 23, 24]. Therefore, the candidate material which has less fragility are desired.

Recent studies suggest that a bond-edge shared honeycomb lattice material based on  $3d^7$   $\text{Co}^{2+}$  ions with a high-spin  $t_{2g}^5 e_g^2$  configuration and a spin-orbit entangled  $J_{\text{eff}} = 1/2$  state can be a good candidate to realized Kitaev

\* These authors contributed equally to this work.

† [ykohama@g.ecc.u-tokyo.ac.jp](mailto:ykohama@g.ecc.u-tokyo.ac.jp)

‡ [w.li@itp.ac.cn](mailto:w.li@itp.ac.cn)

§ [ymatsuda@issp.u-tokyo.ac.jp](mailto:ymatsuda@issp.u-tokyo.ac.jp)

physics [25–28]. Proposed Co-based candidates include  $\text{Na}_2\text{Co}_2\text{TeO}_6$ ,  $(\text{Na},\text{Li})_3\text{Co}_2\text{SbO}_6$ , and  $\text{BaCo}_2(\text{AsO}_4)_2$  [25, 27]. To study the possible intermediate phase under an out-of-plane magnetic field and benchmark against  $\alpha\text{-RuCl}_3$ , we select  $\text{Na}_2\text{Co}_2\text{TeO}_6$  due to its comparable material properties. Both compounds exhibit a double-peak feature in specific heat at zero field, with the low- $T$  peak at  $T_N$  and the higher one around 100 K [29, 30]. Additionally, both of them show the zigzag ordered ground state with M-point peak in the Brillouin zone from the neutron scattering studies [31, 32], and show significant magnetic anisotropy [29, 33, 34].

Despite these similarities, there are notable distinctions between the two compounds. Previous studies have suggested an AFM Kitaev interaction with  $K > 0$  in  $\text{Na}_2\text{Co}_2\text{TeO}_6$  [28, 35–37], which contrasts with the ferromagnetic (FM) coupling characterized by  $K < 0$  revealed in  $\alpha\text{-RuCl}_3$  [14, 20, 38, 39]. Given the presence of AFM Kitaev interaction in this compound, theoretical predictions about the emergence of an intermediate-field quantum spin liquid (QSL) in the AFM Kitaev model subjected to out-of-plane fields [19, 40–43], there is a compelling case for high-field studies on this compound along the  $c$  axis. Experimentally, while prior studies on  $\text{Na}_2\text{Co}_2\text{TeO}_6$  under in-plane fields have unveiled rich quantum spin states and quantum phase transitions [32, 36], investigations under out-of-plane fields have been relatively limited.

In this study, we measured the magnetization ( $M$ ) process of  $\text{Na}_2\text{Co}_2\text{TeO}_6$  under various field angles. When the magnetic field ( $H$ ) is applied along the  $c$ -axis direction, we identified four phase transitions ( $H_c^1$ – $H_c^4$ ) from the  $M$ - $H$  results up to 100 T, which show significant difference from the in-plane magnetic field results. Based on the phase transitions observed in the  $M$ - $H$  curves, we present the low-temperature  $\theta$ - $H$  phase diagram of  $\text{Na}_2\text{Co}_2\text{TeO}_6$ , where  $\theta$  is the angle between the  $c$ -axis and the magnetic field. The  $\theta$ - $H$  phase diagram shows three magnetic phases, similar to the previously reported phase diagram in  $\alpha\text{-RuCl}_3$  [21]. Regardless of the field angle, we observe an AFM phase at low-field region, whose upper boundary shows strong magnetic anisotropy; e.g. the critical fields at  $0^\circ$  and  $75^\circ$  are  $\sim 38$  T and  $\sim 7$  T, respectively. After the AFM order is suppressed by the magnetic field, a partially polarized (PP) paramagnetic phase appears at higher fields. Importantly, when the  $\theta$  is close to  $0^\circ$ , an intermediate-field phase emerges between the transition fields  $H_c^3$  (around 38 T) and  $H_c^4$  (around 82 T). This intermediate phase is suggested to be disordered, as also supported by magnetocaloric effect (MCE) measurements up to 55 T. To explain the observed  $\theta$ - $H$  phase diagram, we propose an effective microscopic spin model with larger  $K > 0$  interaction. Our results indicate that the intermediate quantum disordered phase is very likely a quantum spin liquid (QSL) state, as expected for the AFM Kitaev model under out-of-plane fields [19, 41, 42]. It thus prompts further experimental studies of this phase in  $\text{Na}_2\text{Co}_2\text{TeO}_6$  under high magnetic fields.

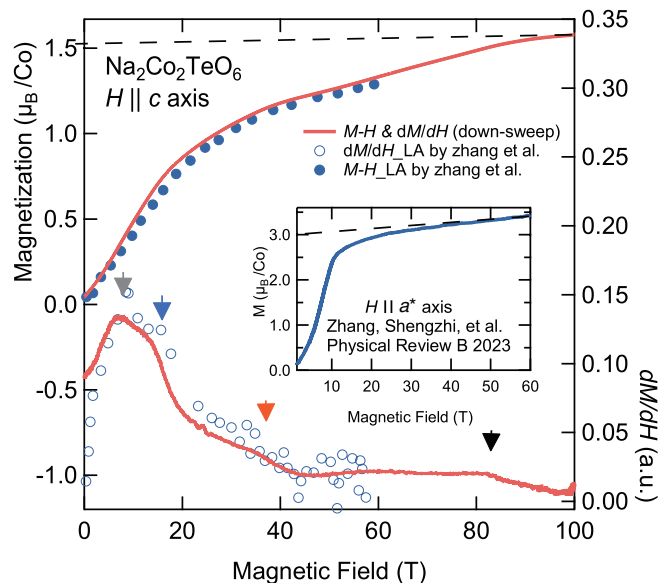


FIG. 1. **Magnetization data measured by the single-turn coil field.** The magnetization and  $dM/dH$  data measured along  $c$ -axis external field up to 100 T. The blue circles represent the magnetization curve up to 60 T from Ref. [34]. The critical fields  $H_c^1$  to  $H_c^4$  are marked by gray, blue, red, and black arrows, respectively. The inset shows the magnetization results under in-plane magnetic field, which is also reported in Ref. [34], where the slope of the black dashed fitting line indicates the van Vleck paramagnetism.

## II. EXPERIMENTAL AND CALCULATED DETAILS

High-quality single crystal of  $\text{Na}_2\text{Co}_2\text{TeO}_6$  were grown by a flux method using a modified from Ref. [28]. We used a platinum crucible instead of an alumina crucible. The temperature and other synthesis sequence is same as the Ref [28]. We obtained dark-red thin single crystals.

The external magnetic fields were generated by vertical-type single-turn coil and non-destructive field generators that are capable of magnetic field up to 102 [44] and 55 T, respectively. The magnetization processes under out-of-plane fields and those at various rotated angles were measured using a 1.6 mm diameter pick-up coil consisting of two small coils compensating for each other [21, 45–47]. A single crystal of  $\text{Na}_2\text{Co}_2\text{TeO}_6$  was employed for the present experiment. To prepare the sample for measurement, it was cut into small honeycomb pieces with a diameter of 1.3 mm. Approximately 20 such chips, each with a thickness of about 0.1 mm, were stacked together to achieve sufficient thickness for measuring the magnetization process in the single-turn coil experiments. Here, we use the same method with our previous work [21] to control the field directions, i.e.  $\theta$  angle. Weak transitions below 50 T were confirmed by non-destructive magnetization measurements. All magnetization measurements were conducted at 4.2 K.

The field dependence of the sample temperature, magnetocaloric effect (MCE), was measured in pulsed magnetic field using a AuGe thin film thermometer [48]. The AuGe film thermometer was directly sputtered on a flat surface of a piece of single crystals ( $2 \times 2 \times 0.1 \text{ mm}^3$ ). The sample was kept in high vacuum condition during the pulsed magnetic fields of 36 ms duration. Because of the weak thermal coupling and limited timescale, the MCE traces,  $T(H)$ , can be considered as adiabatic temperature changes which correspond to isentropic temperature traces as a function of magnetic field [48].

The magnetization process and the values of transition fields under different field angles are calculated by the powerful density matrix renormalization group (DMRG) method [49], where the quantum state can be efficiently expressed as matrix product states (MPS). The DMRG simulations are performed on the cylindrical lattices, where the angle  $\theta$  with respect to  $c$ -axis indicating the direction of field and is represented by  $\cos(\theta)[\sqrt{\frac{1}{3}} - \sqrt{\frac{1-\cos^2(\theta)}{2\cos^2(\theta)}}, \sqrt{\frac{1}{3}}, \sqrt{\frac{1}{3}} + \sqrt{\frac{1-\cos^2(\theta)}{2\cos^2(\theta)}}]$  in the spin space ( $S^x, S^y, S^z$ ). More details of the method and results could be found in Supplementary Note 2.

### III. EXPERIMENTAL RESULTS

In Fig. 1, we present the magnetization process and  $dM/dH$  by the red curves, obtained by the induction method under the out-of-plane ( $c$ -axis) magnetic field up to 100 T. Unlike our previous work [21, 46, 47], here we only show the magnetization data measured during the down-sweep process of the field generated by the single-turn coil. This is because the significant switching electromagnetic noise during the up-sweep field process, which hinders the observation of small signals [44, 46]. Although the inhomogeneity of the magnetic field in the single-turn coil generator might renders down-sweep data invalid, the reliability of the data is confirmed by the perfect reproducibility between the up-sweep and down-sweep data, as demonstrated in Fig. S1. Furthermore, we compare our results with magnetization data up to 60 T from Ref. [34] to calibrate the absolute values. The out-of-plane magnetization process exhibits substantial differences compared to the in-plane magnetization process in the inset of Fig. 1. This indicates significant magnetic anisotropy, consistent with previous  $g$ -factor measurements [36]. At 100 T, the out-of-plane magnetic moment ( $M_c$ ) is approximately  $1.6 \mu_B$ . To contextualize this value, we compare it with the previously reported in-plane saturated magnetic moment ( $M_{ab}$ ), which is  $3 \mu_B$ , as shown in the inset of Fig. 1. Considering the reported in-plane and out-of-plane  $g$ -factors ( $g_{ab}$  and  $g_c$ ) in Ref. [36] as 4.13 and 2.3, respectively, we find  $M_{ab}/g_{ab} \simeq M_c/g_c$ . This suggests that the magnetization saturates at around 100 T under an out-of-plane magnetic field.

Below the saturation field for  $H \parallel c$ , four anomalies are

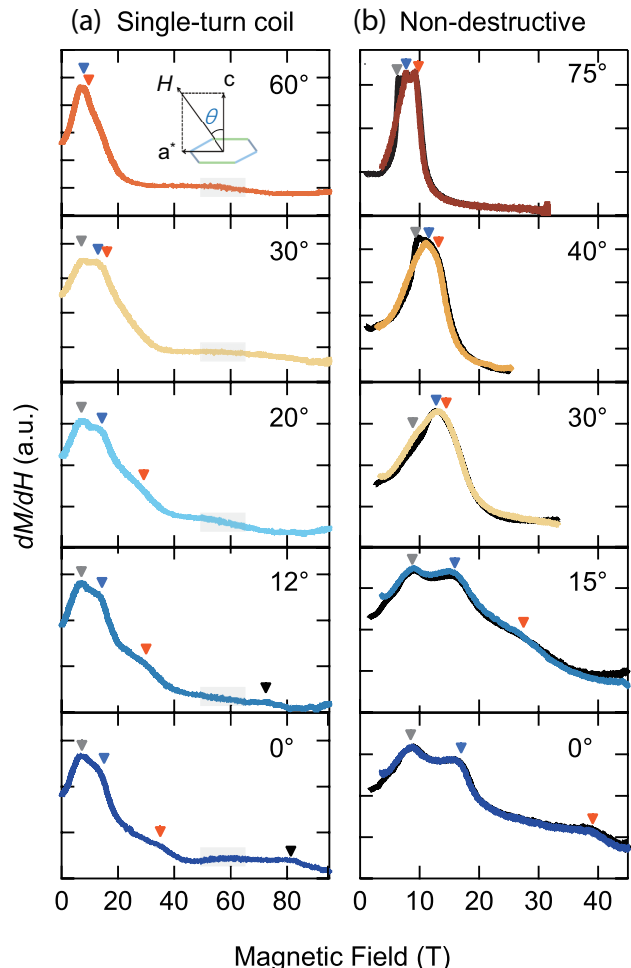


FIG. 2. Measured  $dM/dH$  data versus magnetic fields under various  $\theta$  angles at 4.2 K. (a)  $dM/dH$  curves measured by the single-turn coil; (b)  $dM/dH$  measured under the non-destructive magnetic fields. The color and black curves represent the down- and up-sweep results, respectively. The gray, blue, red, and black arrows also correspond to the transition fields at  $H_c^1$ ,  $H_c^2$ ,  $H_c^3$ , and  $H_c^4$ , as marked in Fig. 1. The inset show the definition of the angles between the magnetic field and  $c$  axis. All of y-axis ( $dM/dH$ ) start from zero. The field independent hump structure marked with gray windows may caused by the experimental errors as shown in Fig. S1.

observed in the  $dM/dH$  curve at 7, 16, 36, and 82 T, respectively. These anomalies are denoted as  $H_c^1$ ,  $H_c^2$ ,  $H_c^3$ , and  $H_c^4$ , and are marked with gray, blue, red, and black arrows in sequence, as shown in Fig. 1. The anomalies at  $H_c^1$  and  $H_c^2$  agree well with previous magnetization reports in Refs. [34]. In this work, we focus on the observation of the other two anomalies,  $H_c^3$  and  $H_c^4$ . Additionally, to ensure the robustness of the results, we conducted two experiments at  $\theta \simeq 0^\circ$ , confirming that the anomaly at 82 T is not introduced by artificial reasons, as shown in Fig. S1.

To investigate the magnetic anisotropy of

$\text{Na}_2\text{Co}_2\text{TeO}_6$ , we conducted measurements of the magnetization process up to 100 T along different field directions, i.e.,  $\theta \simeq 0^\circ, 12^\circ, 20^\circ, 30^\circ$ , and  $60^\circ$ , using the single-turn coil field generator. The results are shown in Fig. 2(a). To check the reproducibility of our magnetization data, a non-destructive field experiment was also performed up to 50 T. The results are presented in Fig. 2(b) for  $\theta \simeq 0^\circ, 15^\circ, 30^\circ, 40^\circ$ , and  $75^\circ$ . The anomalies at  $H_c^1, H_c^2, H_c^3$ , and  $H_c^4$  are marked with gray, blue, red, and black triangles, respectively.

As shown in Fig. 2(a) and (b), the anomalies at  $H_c^1$  and  $H_c^2$  are almost  $\theta$ -independent, while those at  $H_c^3$  and  $H_c^4$  exhibit significant changes with different  $\theta$  angles. At  $\theta \simeq 0^\circ$ ,  $H_c^3$  observed in the single-turn coil system is  $\sim 36$  T, which is almost the same as the value,  $\sim 38$  T, obtained with the non-destructive magnet.  $H_c^4$  is  $\sim 82$  T, as also shown in Fig. 1. At  $\theta \simeq 12^\circ \pm 5^\circ$ ,  $H_c^3$  and  $H_c^4$  decreases to  $\sim 30$  T and  $\sim 72$  T, respectively. Above  $15^\circ$ ,  $H_c^4$  becomes difficult to be distinguished. On the other hand,  $H_c^3$  continues to decrease with increasing  $\theta$  angles, and eventually almost merges with  $H_c^1$  and  $H_c^2$  at high  $\theta$  angles (c.f.,  $60^\circ$  in Fig. 2(a) and  $75^\circ$  in Fig. 2(b)). Notably,  $H_c^1, H_c^2$ , and  $H_c^3$  are 6.3, 7.6, and 10 T, respectively, at  $\theta \simeq 75^\circ$ , which is almost the same as the previous in-plane results [34]. The  $dM/dH$  results shown in Fig. 2(a) and (b) exhibit excellent agreement with each other.

To track the temperature dependence of the phase boundary,  $H_c(T)$ , we also measured the magnetocaloric effect (MCE) of  $\text{Na}_2\text{Co}_2\text{TeO}_6$  for  $H \parallel c$  up to 55 T, as the dip in MCE curves corresponds to the field-induced phase transition and is used to map out the temperature-field phase boundaries [50–52]. As shown in Fig. 3, the isentrope curve starting from 5 K at zero field shows three local minima at 4, 16, and 37 T, as indicated by the gray, blue and red arrows, respectively. Such minima correspond to the observed magnetization anomalies at  $H_c^1, H_c^2$ , and  $H_c^3$  as shown in Fig. 2(a) and (b) at  $\theta \simeq 0^\circ$ . As the temperature increases, these minima shift toward lower fields, suggesting phase transitions are associated with changes in spin configurations. Above  $T_N$  ( $\sim 28$  K), the dip structure correlated to  $H_c^3$  disappears, and the isentrope curves show a peculiar upward feature. Here, we deduce that the minima pointed by the orange arrow smoothly connects to the zero-field transition temperature of  $T_N$  as well as to the zero-temperature phase boundary of  $H_c^3$  as seen in the dashed curve of Fig. 3. We also note the isentrope curves show the dome structures when magnetic field is larger than  $H_c^3$  or temperature is higher than  $T_N$ . This indicates the possible emergence of additional dip structures of the isentrope curves at high magnetic field.

#### IV. DISCUSSIONS

Previous studies [33, 34, 53] have reported that  $H_c^1$  and  $H_c^2$  are related to the re-arrangement of AFM order. Specifically, we find  $H_c^1$  is associated with a first-

order phase transition at large angles, i.e.  $\theta > 30^\circ$ . This is evidenced by the significant hysteresis between the up- and down-sweep  $dM/dH$  curves. At small angles, the hysteresis become difficult to distinguish. This may be caused by the path difference of phase transition in the parameter space. In our results with different angles, the values of  $H_c^1$  and  $H_c^2$  does not show large angle dependence that is consistent with Ref. [34]. On the other hand,  $H_c^3$  exhibits significant magnetic anisotropy, as shown in Fig. 2. At  $\theta \simeq 60^\circ$  or  $75^\circ$ ,  $H_c^3$  is only  $\sim 10$  T, while it increases to  $\sim 38$  T at  $\theta \simeq 0^\circ$ . According to the MCE results in Fig. 3, AFM order is suppressed at  $H_c^3$  under the out-of-plane field, as indicated by the monotonic decrease in  $H_c^3$  with increasing temperature and its connection to  $T_N$  at zero field. The monotonic suppression of  $H_c^3$  in the T-H phase diagram is similar with the one for in-plane magnetic field [34]. Such result implies the low-temperature phase above  $H_c^3$  is quantum disordered, consistent with previous specific heat results, where the specific heat peak representing the magnetic order could still be observed under the out-of-plane field up to 19.3 T although it has been significantly suppressed [29].

It is noteworthy that after the magnetic order is sup-

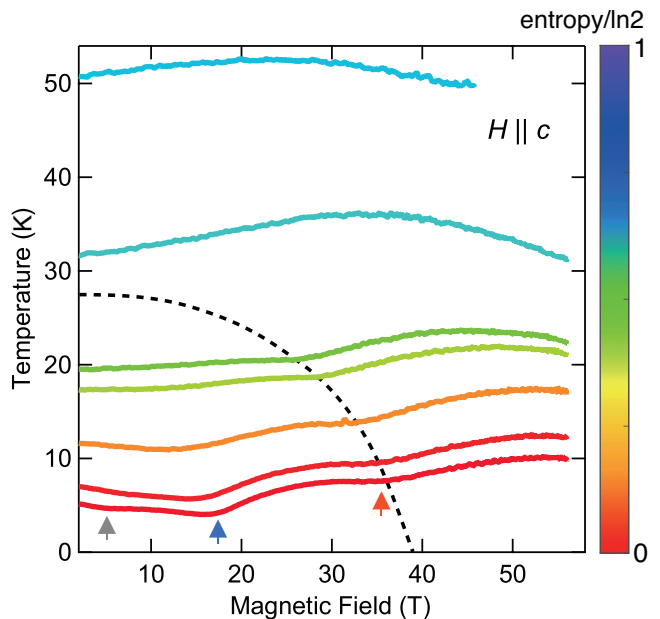


FIG. 3. **Magnetocaloric Effect measured under the non-destructive magnetic fields.** The field was applied to the  $c$ -axis ( $\theta = 0^\circ$ ). Three critical fields,  $H_c^1, H_c^2$ , and  $H_c^3$ , are marked with gray, blue, and red arrows. The finite-temperature phase boundaries originating from  $T_N$  at zero field and converging towards  $H_c^3$  signify the suppression of AFM ordered phases, as depicted by the black dashed curve serving as the guide for the eye. The color of entropy at different temperatures are determined by the previous reported specific heat results [29].



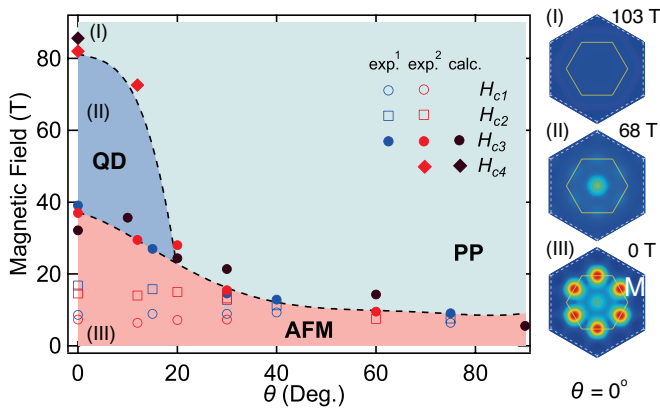


FIG. 4. **Field-angle phase diagram determined by the low temperature experiments and calculations.** The experimental critical fields are obtained by the magnetization measurement in Fig. 2. “exp.<sup>1</sup>” and “exp.<sup>2</sup>” represent the single-turn coil and non-destructive field data. We use open circle, open square, solid circle, and solid rhombus to mark the transitions  $H_c^1$ ,  $H_c^2$ ,  $H_c^3$ , and  $H_c^4$ . The results from DMRG calculations are also indicated by solid circles and diamonds. Three phases, i.e., AFM, intermediate quantum disordered (QD), and PP are separated by the dashed curves which serve as guides for the eye. Panels (I-III) in the right side show the static spin structure factors under three field strength at  $\theta = 0^\circ$ , demonstrating the distinct characteristics of these three phases.

pressed at  $H_c^3$ , a new phase transition is observed at  $H_c^4 \simeq 82$  T for  $H \parallel c$ , defining a saturation field. Therefore, we concluded that the phase between  $H_c^3$  and  $H_c^4$  is an intermediate phase and show disordered feature. As the intermediate regime across a wide range of external field, i.e. from 38 to 82 T, it is very robust against magnetic field. Such behavior is distinct from the field-induced paramagnetic phase, which should be polarized by the magnetic field immediately. Therefore, there exists strong quantum fluctuation in this intermediate disordered phase, which supports that it is a QSL phase [54]. Such MCE behavior is also consistent with the simulated one previously proposed for  $\alpha$ -RuCl<sub>3</sub> model [22, 55, 56], e.g., a dip feature observed in isentropes is found to be relatively weak near the transition point from AFM to the intermediate quantum disordered phase [55], e.g., near  $H_c^3$  (see Fig. 3), which suggests a small entropy change. This can be ascribed to the relatively large Kitaev interaction (about 300 K) and low temperature scale associated with the intermediate-field regime [22, 55, 56]. Consequently, the entropy differences between different phases are rather limited in the relevant temperature window. We find this phase only emerges at  $\theta$  less than  $12^\circ$ , which is also very similar to the possible intermediate QSL state previously reported in  $\alpha$ -RuCl<sub>3</sub> experiments [21]. To clarify this special intermediate phase, the critical fields are summarized in Fig. 4 with a  $\theta$ - $H$  phase diagram.

The establishment of a microscopic spin model is es-

sential for elucidating the phases and phase transitions induced by an external field. In previous neutron studies, C. Kim et al. proposed that the Kitaev interaction in Na<sub>2</sub>Co<sub>2</sub>TeO<sub>6</sub> is more reasonably attributed to be AFM [28]. Certain models containing the AFM Kitaev interactions have been contemplated [28, 37, 57], which are constructed based on the  $K$ - $\Gamma$ - $\Gamma'$ - $J$  model,  $H = \sum_{\langle i,j \rangle_\gamma} [K S_i^\gamma S_j^\gamma + J \mathbf{S}_i \cdot \mathbf{S}_j + \Gamma(S_i^\alpha S_j^\beta + S_i^\beta S_j^\alpha) + \Gamma'(S_i^\gamma S_j^\alpha + S_i^\alpha S_j^\gamma + S_i^\beta S_j^\gamma)]$ , for Kitaev magnets. These models share several common features: the Kitaev ( $K$ ) interaction, which defines the energy scale, is ranging from 1.0 to 3.5 meV; and  $\Gamma'/|K|$  is approximately 0.6. In addition, there are also other proposed models based on ferromagnetic (FM) Kitaev interaction or XXZ  $J_1$ - $J_3$  model [28, 32, 35, 37]. Thus the microscopic spin model of Na<sub>2</sub>Co<sub>2</sub>TeO<sub>6</sub>, including both the sign of  $K$  and its interaction form, remains undetermined. To address this, we conducted DMRG method to simulate the magnetization process. The calculated magnetization curves with these previously proposed models under in-plane and out-of-plane fields are shown in Fig. S2. We find all of these calculated results show significant differences compared to the experimental magnetization process. The primary discrepancy arises from the saturated field of Na<sub>2</sub>Co<sub>2</sub>TeO<sub>6</sub> under the out-of-plane field. The calculated magnetization saturates below 50 T based on the previously proposed models, while our experimental results demonstrate that the saturation field is 82 T. Therefore, understanding the magnetic interactions within Na<sub>2</sub>Co<sub>2</sub>TeO<sub>6</sub> is of particular interest, especially given the insights provided by recent high-field measurements.

Inspired by the similarities between Na<sub>2</sub>Co<sub>2</sub>TeO<sub>6</sub> and  $\alpha$ -RuCl<sub>3</sub>, such as the zigzag ground state [31, 32] and double-peak specific heat [29, 30], as well as the similar  $\theta$ - $H$  phase diagram obtained in this study, we conjecture that the microscopic spin models of these two materials share a similar form. Within the framework of  $K > 0$  [28], we firstly transform the previously proposed spin model for  $\alpha$ -RuCl<sub>3</sub> [20, 21] by using the Chaloupka-Khaliullin transformation [58], and obtain an effective Hamiltonian with AFM Kitaev interaction:  $K = 19$  meV,  $J = -0.9|K|$ ,  $\Gamma = -0.65|K|$ , and  $\Gamma' = 0.36|K|$ .

Based on this newly proposed spin model, we calculate the magnetization process under different field directions, with results consistent with experimental data (see Fig. S3). Moreover, we have determined the critical fields from our calculations and also presented them in Fig. 4, which show good agreement with the experimental results. Moreover, with the above model, we further calculate the spin structure factors  $S(\mathbf{q})$  under various out-of-plane fields. At zero and low fields, the  $S(\mathbf{q})$  show peaks at M points in the Brillouin zone, indicating the antiferromagnetic zigzag order, which agrees well with neutron experimental results [32, 59]. With the increment of the fields, the M-point intensity diminishes in the intermediate-field regime, which signifies the presence of quantum spin disorder in such phase captured

in our experiments. We also calculate the corresponding MCE curves under the  $c$ -axis fields up to 100 T based on this effective model, as shown in Fig. S4. In the low-field region, i.e. less than 55 T, the calculated curves show consistency with the experimental results, which further implies the validity of the model. Particularly, the dome structure of MCE results when temperature is higher than  $T_N$  or field is larger than  $H_c^3$ , as shown in Fig. S4, are also reproduced in the calculated MCE results.

In short summary, here we note that both the experimental and calculated results support that it is a quantum disordered phase with strong quantum fluctuation in the intermediate-field regime. The emergence of this quantum disordered phase in  $\text{Na}_2\text{Co}_2\text{TeO}_6$  is corroborated by the microscopic spin model with a large AFM Kitaev interaction. This indicates that the quantum disordered intermediate-field phase is most likely caused by the intrinsic properties of the AFM Kitaev term, and such intermediate regime is possibly corresponding to a field-induced QSL in the AFM Kitaev model under the application of magnetic fields. It warrants further in-depth investigation into whether this possible QSL phase is gapped or gapless, which have been discussed in previous theoretical studies [42, 60].

## V. CONCLUSION

We have constructed the field-angle phase diagram of  $\text{Na}_2\text{Co}_2\text{TeO}_6$  through magnetization and MCE measurements at high magnetic field. At low temperatures,  $\text{Na}_2\text{Co}_2\text{TeO}_6$  enters an AFM phase below 38 T, showing strong magnetic anisotropy. After the AFM order is suppressed by an external field, the system enters a PP phase for  $\theta > 12^\circ$ . Notably, at smaller  $\theta$ , an intermediate disordered phase emerges, determined by the critical fields  $H_c^3$  and  $H_c^4$  at  $\theta \approx 0^\circ$  and  $12^\circ$ . This phase diagram is similar to that of  $\alpha\text{-RuCl}_3$  [21]. MCE measurements provide evidence that this intermediate phase is disordered, which was not experimentally proven for  $\alpha\text{-RuCl}_3$  previously [21]. The high upper field boundary of this phase, i.e.  $H_c^4 \simeq 82$  T, indicates that this intermediate phase is very robust against the application of a magnetic field, which further suggests the presence of strong quantum fluctuations and a

possible connection to the QSL state in field-induced AFM Kitaev model. Combining experimental data with DMRG calculations, we propose a microscopic spin model with a large Kitaev interaction, which places  $\text{Na}_2\text{Co}_2\text{TeO}_6$  as a proximate dual Kitaev material to  $\alpha\text{-RuCl}_3$ , through an unitary transformation. This model explains the anisotropy of the AFM phase in  $\text{Na}_2\text{Co}_2\text{TeO}_6$  and the quantum disordered intermediate phase under a perpendicular field. However, the model struggles with the low-field isotropic phase transition, likely influenced by three-dimensional interactions not included in the DMRG calculations based on the two-dimensional spin model. The broad magnetic isotropic hump structures in experimental  $dM/dH$  data (marked by gray windows in Fig. 2(a)) also remain unclear, which may only due to the experimental error as shown in Fig. S1(a). Compared to  $\alpha\text{-RuCl}_3$ ,  $\text{Na}_2\text{Co}_2\text{TeO}_6$  is more robust and less susceptible to damage from external stress, allowing various measurement methods under high magnetic fields. This provides a better platform to understand the nature of the possible intermediate-field QSL phase under an out-of-plane magnetic field.

## Acknowledgements

X.-G.Z. thank Jian Yan, Fengfeng Song and Weiliang Yao for fruitful discussions. This work was partly supported by JSPS KAKENHI, Grant-in-Aid for Scientific Research (Nos. JP23H04859, JP23H04860 and JP22H00104). X.-G.Z. and Y.H.M. were funded by JSPS KAKENHI NO. 22F22332 and ENHI Challenging Research (Pioneering) No. 20K20521. H.L. and W.L. were supported by the National Natural Science Foundation of China (Grant Nos. 12222412, 11834014, 11974036, and 12047503), CAS Project for Young Scientists in Basic Research (Grant No. YSBR-057), and China National Postdoctoral Program for Innovative Talents (Grant No. BX20220291). Work at SNU was supported by the Leading Researcher Program of the National Research Foundation of Korea (Grant No. 2020R1A3B2079375).

*Note added.*— After completing the current work, we became aware of a recent study by Zhang et al. [61], where the authors also observed the existence of  $H_c^3$ , which is consistent with our findings.

- 
- [1] A. Kitaev, Anyons in an exactly solved model and beyond, *Ann. Phys.* **321**, 2 (2006), january Special Issue.
  - [2] C. Nayak, S. H. Simon, A. Stern, M. Freedman, and S. Das Sarma, Non-abelian anyons and topological quantum computation, *Rev. Mod. Phys.* **80**, 1083 (2008).
  - [3] V. Lahtinen and J. K. Pachos, A Short Introduction to Topological Quantum Computation, *SciPost Phys.* **3**, 021 (2017).
  - [4] G. Jackeli and G. Khaliullin, Mott insulators in the

strong spin-orbit coupling limit: From Heisenberg to a quantum compass and Kitaev models, *Phys. Rev. Lett.* **102**, 017205 (2009).

- [5] J. Chaloupka, G. Jackeli, and G. Khaliullin, Kitaev-Heisenberg model on a honeycomb lattice: Possible exotic phases in iridium oxides  $\text{A}_2\text{IrO}_3$ , *Phys. Rev. Lett.* **105**, 027204 (2010).
- [6] H. Takagi, T. Takayama, G. Jackeli, G. Khaliullin, and S. E. Nagler, Concept and realization of Kitaev quantum

- spin liquids, *Nat. Rev. Phys.* **1**, 264 (2019).
- [7] Y. Kubota, H. Tanaka, T. Ono, Y. Narumi, and K. Kindo, Successive magnetic phase transitions in  $\alpha$ - $\text{RuCl}_3$ : XY-like frustrated magnet on the honeycomb lattice, *Phys. Rev. B* **91**, 094422 (2015).
- [8] R. D. Johnson, S. C. Williams, A. A. Haghighirad, J. Singleton, V. Zapf, P. Manuel, I. I. Mazin, Y. Li, H. O. Jeschke, R. Valentí, and R. Coldea, Monoclinic crystal structure of  $\alpha$ - $\text{RuCl}_3$  and the zigzag antiferromagnetic ground state, *Phys. Rev. B* **92**, 235119 (2015).
- [9] Y. Kasahara, T. Ohnishi, Y. Mizukami, O. Tanaka, S. Ma, K. Sugii, N. Kurita, H. Tanaka, J. Nasu, Y. Motome, T. Shibauchi, and Y. Matsuda, Majorana quantization and half-integer thermal quantum Hall effect in a Kitaev spin liquid, *Nature* **559**, 227 (2018).
- [10] A. Banerjee, C. A. Bridges, J. Q. Yan, A. A. Aczel, L. Li, M. B. Stone, G. E. Granroth, M. D. Lumsden, Y. Yiu, J. Knolle, S. Bhattacharjee, D. L. Kovrizhin, R. Moessner, D. A. Tennant, D. G. Mandrus, and S. E. Nagler, Proximate Kitaev quantum spin liquid behaviour in a honeycomb magnet, *Nat. Mater.* **15**, 733 (2016).
- [11] A. Banerjee, J. Yan, J. Knolle, C. A. Bridges, M. B. Stone, M. D. Lumsden, D. G. Mandrus, D. A. Tennant, R. Moessner, and S. E. Nagler, Neutron scattering in the proximate quantum spin liquid  $\alpha$ - $\text{RuCl}_3$ , *Science* **356**, 1055 (2017).
- [12] S.-H. Do, S.-Y. Park, J. Yoshitake, J. Nasu, Y. Motome, Y. S. Kwon, D. T. Adroja, D. J. Voneshen, K. Kim, T.-H. Jang, J.-H. Park, K.-Y. Choi, and S. Ji, Majorana fermions in the Kitaev quantum spin system  $\alpha$ - $\text{RuCl}_3$ , *Nat. Phys.* **13**, 1079 (2017).
- [13] A. Banerjee, P. Lampen-Kelley, J. Knolle, C. Balz, A. Aczel, B. Winn, Y. Liu, D. Pajerowski, J. Yan, C. A. Bridges, A. T. Savici, B. C. Chakoumakos, M. D. Lumsden, D. A. Tennant, R. Moessner, D. G. Mandrus, and S. E. Nagler, Excitations in the field-induced quantum spin liquid state of  $\alpha$ - $\text{RuCl}_3$ , *npj Quant. Mater.* **3**, 8 (2018).
- [14] S. M. Winter, K. Riedl, D. Kaib, R. Coldea, and R. Valentí, Probing  $\alpha$ - $\text{RuCl}_3$  beyond magnetic order: Effects of temperature and magnetic field, *Phys. Rev. Lett.* **120**, 077203 (2018).
- [15] O. Tanaka, Y. Mizukami, R. Harasawa, K. Hashimoto, K. Hwang, N. Kurita, H. Tanaka, S. Fujimoto, Y. Matsuda, E. Moon, and T. Shibauchi, Thermodynamic evidence for a field-angle-dependent majorana gap in a kitaev spin liquid, *Nature Physics* **18**, 429 (2022).
- [16] K. Imamura, S. Suetsugu, Y. Mizukami, Y. Yoshida, K. Hashimoto, K. Ohtsuka, Y. Kasahara, N. Kurita, H. Tanaka, P. Noh, J. Nasu, E.-G. Moon, Y. Matsuda, and T. Shibauchi, Majorana-fermion origin of the planar thermal hall effect in the kitaev magnet  $\alpha$ - $\text{RuCl}_3$ , *Science Advances* **10**, eadk3539 (2024).
- [17] S. Bachus, D. A. S. Kaib, Y. Tokiwa, A. Jesche, V. Tsurkan, A. Loidl, S. M. Winter, A. A. Tsirlin, R. Valentí, and P. Gegenwart, Thermodynamic perspective on field-induced behavior of  $\alpha$ - $\text{RuCl}_3$ , *Phys. Rev. Lett.* **125**, 097203 (2020).
- [18] K. Riedl, Y. Li, S. M. Winter, and R. Valentí, Sawtooth torque in anisotropic  $j_{\text{eff}} = 1/2$  magnets: Application to  $\alpha$ - $\text{RuCl}_3$ , *Phys. Rev. Lett.* **122**, 197202 (2019).
- [19] J. S. Gordon, A. Catuneanu, E. S. Sørensen, and H.-Y. Kee, Theory of the field-revealed Kitaev spin liquid, *Nat. Commun.* **10**, 2470 (2019).
- [20] H. Li, H.-K. Zhang, J. Wang, H.-Q. Wu, Y. Gao, D.-W. Qu, Z.-X. Liu, S.-S. Gong, and W. Li, Identification of magnetic interactions and high-field quantum spin liquid in  $\alpha$ - $\text{RuCl}_3$ , *Nat. Commun.* **12**, 4007 (2021).
- [21] X.-G. Zhou, H. Li, Y. H. Matsuda, A. Matsuo, W. Li, N. Kurita, G. Su, K. Kindo, and H. Tanaka, Possible intermediate quantum spin liquid phase in  $\alpha$ - $\text{rucl}_3$  under high magnetic fields up to 100 T, *Nature Communications* **14**, 5613 (2023).
- [22] H. Li, W. Li, and G. Su, High-field quantum spin liquid transitions and angle-field phase diagram of the Kitaev magnet  $\alpha$ - $\text{RuCl}_3$ , *Phys. Rev. B* **107**, 115124 (2023).
- [23] K. A. Modic, R. D. McDonald, J. P. C. Ruff, M. D. Bachmann, Y. Lai, J. C. Palmstrom, D. Graf, M. K. Chan, F. F. Balakirev, J. B. Betts, G. S. Boebinger, M. Schmidt, M. J. Lawler, D. A. Sokolov, P. J. W. Moll, B. J. Ramshaw, and A. Shekhter, Scale-invariant magnetic anisotropy in  $\text{RuCl}_3$  at high magnetic fields, *Nat. Phys.* **17**, 240 (2021).
- [24] H. B. Cao, A. Banerjee, J.-Q. Yan, C. A. Bridges, M. D. Lumsden, D. G. Mandrus, D. A. Tennant, B. C. Chakoumakos, and S. E. Nagler, Low-temperature crystal and magnetic structure of  $\alpha$ - $\text{RuCl}_3$ , *Phys. Rev. B* **93**, 134423 (2016).
- [25] R. Sano, Y. Kato, and Y. Motome, Kitaev-Heisenberg hamiltonian for high-spin  $d^7$  mott insulators, *Phys. Rev. B* **97**, 014408 (2018).
- [26] H. Liu, J. c. v. Chaloupka, and G. Khaliullin, Kitaev spin liquid in  $3d$  transition metal compounds, *Phys. Rev. Lett.* **125**, 047201 (2020).
- [27] H. Liu and G. Khaliullin, Pseudospin exchange interactions in  $d^7$  cobalt compounds: Possible realization of the Kitaev model, *Phys. Rev. B* **97**, 014407 (2018).
- [28] C. Kim, J. Jeong, G. Lin, P. Park, T. Masuda, S. Asai, S. Itoh, H.-S. Kim, H. Zhou, J. Ma, and J.-G. Park, Antiferromagnetic Kitaev interaction in  $J_{\text{eff}} = 1/2$  cobalt honeycomb materials  $\text{Na}_3\text{Co}_2\text{SbO}_6$  and  $\text{Na}_2\text{Co}_2\text{TeO}_6$ , *J. Phys.: Condens. Matter* **34**, 045802 (2021).
- [29] H. Yang, C. Kim, Y. Choi, J. H. Lee, G. Lin, J. Ma, M. Kratochvílová, P. Proschek, E.-G. Moon, K. H. Lee, Y. S. Oh, and J.-G. Park, Significant thermal Hall effect in the  $3d$  cobalt Kitaev system  $\text{Na}_2\text{Co}_2\text{TeO}_6$ , *Phys. Rev. B* **106**, L081116 (2022).
- [30] W. Yao and Y. Li, Ferrimagnetism and anisotropic phase tunability by magnetic fields in  $\text{Na}_2\text{Co}_2\text{TeO}_6$ , *Phys. Rev. B* **101**, 085120 (2020).
- [31] A. K. Bera, S. M. Yusuf, A. Kumar, and C. Ritter, Zigzag antiferromagnetic ground state with anisotropic correlation lengths in the quasi-two-dimensional honeycomb lattice compound  $\text{Na}_2\text{Co}_2\text{TeO}_6$ , *Phys. Rev. B* **95**, 094424 (2017).
- [32] W. Yao, K. Iida, K. Kamazawa, and Y. Li, Excitations in the ordered and paramagnetic states of honeycomb magnet  $\text{Na}_2\text{Co}_2\text{TeO}_6$ , *Phys. Rev. Lett.* **129**, 147202 (2022).
- [33] G. Xiao, Z. Xia, Y. Song, and L. Xiao, Magnetic properties and phase diagram of quasi-two-dimensional  $\text{Na}_2\text{Co}_2\text{TeO}_6$  single crystal under high magnetic field, *Journal of Physics: Condensed Matter* **34**, 075801 (2021).
- [34] S. Zhang, S. Lee, A. J. Woods, W. K. Peria, S. M. Thomas, R. Movshovich, E. Brosha, Q. Huang, H. Zhou, V. S. Zapf, and M. Lee, Electronic and magnetic phase diagrams of the Kitaev quantum spin liquid candidate  $\text{Na}_2\text{Co}_2\text{TeO}_6$ , *Phys. Rev. B* **108**, 064421 (2023).
- [35] M. Songvilay, J. Robert, S. Petit, J. A. Rodriguez-Rivera,

- W. D. Ratcliff, F. Damay, V. Balédent, M. Jiménez-Ruiz, P. Lejay, E. Pachoud, A. Hadj-Azzem, V. Simonet, and C. Stock, Kitaev interactions in the co honeycomb antiferromagnets  $\text{Na}_3\text{Co}_2\text{SbO}_6$  and  $\text{Na}_2\text{Co}_2\text{TeO}_6$ , *Phys. Rev. B* **102**, 224429 (2020).
- [36] G. Lin, J. Jeong, C. Kim, Y. Wang, Q. Huang, T. Masuda, S. Asai, S. Itoh, G. Günther, M. Russina, Z. Lu, J. Sheng, L. Wang, J. Wang, G. Wang, Q. Ren, C. Xi, W. Tong, L. Ling, Z. Liu, L. Wu, J. Mei, Z. Qu, H. Zhou, X. Wang, J.-G. Park, Y. Wan, and J. Ma, Field-induced quantum spin disordered state in spin-1/2 honeycomb magnet  $\text{Na}_2\text{Co}_2\text{TeO}_6$ , *Nat. Commun.* **12**, 5559 (2021).
- [37] A. M. Samarakoon, Q. Chen, H. Zhou, and V. O. Garlea, Static and dynamic magnetic properties of honeycomb lattice antiferromagnets  $\text{Na}_2\text{M}_2\text{TeO}_6$ ,  $m = \text{Co}$  and  $\text{ni}$ , *Phys. Rev. B* **104**, 184415 (2021).
- [38] K. Ran, J. Wang, W. Wang, Z.-Y. Dong, X. Ren, S. Bao, S. Li, Z. Ma, Y. Gan, Y. Zhang, J. T. Park, G. Deng, S. Danilkin, S.-L. Yu, J.-X. Li, and J. Wen, Spin-wave excitations evidencing the Kitaev interaction in single crystalline  $\alpha\text{-RuCl}_3$ , *Phys. Rev. Lett.* **118**, 107203 (2017).
- [39] J. A. Sears, L. E. Chern, S. Kim, P. J. Bereciartua, S. Francoual, Y. B. Kim, and Y.-J. Kim, Ferromagnetic Kitaev interaction and the origin of large magnetic anisotropy in  $\alpha\text{-RuCl}_3$ , *Nat. Phys.* **16**, 837 (2020).
- [40] S. Liang, M.-H. Jiang, W. Chen, J.-X. Li, and Q.-H. Wang, Intermediate gapless phase and topological phase transition of the Kitaev model in a uniform magnetic field, *Phys. Rev. B* **98**, 054433 (2018).
- [41] C. Hickey and S. Trebst, Emergence of a field-driven U(1) spin liquid in the Kitaev honeycomb model, *Nat. Commun.* **10**, 530 (2019).
- [42] N. D. Patel and N. Trivedi, Magnetic field-induced intermediate quantum spin liquid with a spinon fermi surface, *Proceedings of the National Academy of Sciences* **116**, 12199 (2019).
- [43] M.-H. Jiang, S. Liang, W. Chen, Y. Qi, J.-X. Li, and Q.-H. Wang, Tuning topological orders by a conical magnetic field in the Kitaev model, *Phys. Rev. Lett.* **125**, 177203 (2020).
- [44] N. Miura, T. Osada, and S. Takeyama, Research in super-high pulsed magnetic fields at the megagauss laboratory of the university of tokyo, *Journal of low temperature physics* **133**, 139 (2003).
- [45] S. Takeyama, R. Sakakura, Y. H. Matsuda, A. Miyata, and M. Tokunaga, Precise magnetization measurements by parallel self-compensated induction coils in a vertical single-turn coil up to 103 T, *J. Phys. Soc. Jap.* **81**, 014702 (2012).
- [46] Y. H. Matsuda, N. Abe, S. Takeyama, H. Kageyama, P. Corboz, A. Honecker, S. R. Manmana, G. R. Foltin, K. P. Schmidt, and F. Mila, Magnetization of  $\text{SrCu}_2(\text{BO}_3)_2$  in ultrahigh magnetic fields up to 118 T, *Phys. Rev. Lett.* **111**, 137204 (2013).
- [47] X.-G. Zhou, Y. Yao, Y. H. Matsuda, A. Ikeda, A. Matsuo, K. Kindo, and H. Tanaka, Particle-hole symmetry breaking in a spin-dimer system  $\text{TiCuCl}_3$  observed at 100 T, *Phys. Rev. Lett.* **125**, 267207 (2020).
- [48] T. Kihara, Y. Kohama, Y. Hashimoto, S. Katsumoto, and M. Tokunaga, Adiabatic measurements of magneto-caloric effects in pulsed high magnetic fields up to 55 t, *Review of Scientific Instruments* **84**, doi.org/10.1063/1.4811798 (2013).
- [49] S. R. White, Density matrix formulation for quantum renormalization groups, *Phys. Rev. Lett.* **69**, 2863 (1992).
- [50] Y. Kohama, H. Ishikawa, A. Matsuo, K. Kindo, N. Shannon, and Z. Hiroi, Possible observation of quantum spin-nematic phase in a frustrated magnet, *Proceedings of the National Academy of Sciences* **116**, 10686 (2019).
- [51] T. Nomura, Y. Skourski, D. L. Quintero-Castro, A. A. Zvyagin, A. V. Suslov, D. Gorbunov, S. Yasin, J. Wosnitzer, K. Kindo, A. T. M. N. Islam, B. Lake, Y. Kohama, S. Zherlitsyn, and M. Jaime, Enhanced spin correlations in the bose-einstein condensate compound  $\text{Sr}_3\text{Cr}_2\text{O}_8$ , *Phys. Rev. B* **102**, 165144 (2020).
- [52] Z. Wang, M. Schmidt, A. Loidl, J. Wu, H. Zou, W. Yang, C. Dong, Y. Kohama, K. Kindo, D. I. Gorbunov, S. Niesen, O. Breunig, J. Engelmayer, and T. Lorenz, Quantum critical dynamics of a heisenberg-ising chain in a longitudinal field: Many-body strings versus fractional excitations, *Phys. Rev. Lett.* **123**, 067202 (2019).
- [53] H. Takeda, J. Mai, M. Akazawa, K. Tamura, J. Yan, K. Moovendaran, K. Raju, R. Sankar, K.-Y. Choi, and M. Yamashita, Planar thermal hall effects in the kitaev spin liquid candidate  $\text{na}_2\text{co}_2\text{teo}_6$ , *Phys. Rev. Res.* **4**, L042035 (2022).
- [54] Y. Zhou, K. Kanoda, and T.-K. Ng, Quantum spin liquid states, *Reviews of Modern Physics* **89**, 025003 (2017).
- [55] H. Li, H.-K. Zhang, J. Wang, H.-Q. Wu, Y. Gao, D.-W. Qu, Z.-X. Liu, S.-S. Gong, and W. Li, Identification of magnetic interactions and high-field quantum spin liquid in  $\alpha\text{-RuCl}_3$ , *Nat. Commun.* **12**, 4007 (2021).
- [56] S.-Y. Yu, H. Li, Q.-R. Zhao, Y. Gao, X.-Y. Dong, Z.-X. Liu, W. Li, and S.-S. Gong, Nematic chiral spin liquid in a kitaev magnet under external magnetic field, arXiv preprint arXiv:2304.00555 (2023).
- [57] G. Lin, Q. Zhao, G. Li, M. Shu, Y. Ma, J. Jiao, Q. Huang, J. Sheng, A. Kolesnikov, L. Li, L. Wu, X. Wang, H. Zhou, Z. Liu, and J. Ma, Evidence for field induced quantum spin liquid behavior in a spin-1/2 honeycomb magnet (2022).
- [58] J. Chaloupka and G. Khaliullin, Hidden symmetries of the extended Kitaev-Heisenberg model: Implications for the honeycomb-lattice iridates  $\text{A}_2\text{IrO}_3$ , *Phys. Rev. B* **92**, 024413 (2015), arXiv:1502.02587 [cond-mat.str-el].
- [59] E. Lefrançois, M. Songvilay, J. Robert, G. Nataf, E. Jordan, L. Chaix, C. V. Colin, P. Lejay, A. Hadj-Azzem, R. Ballou, and V. Simonet, Magnetic properties of the honeycomb oxide  $\text{Na}_2\text{Co}_2\text{TeO}_6$ , *Phys. Rev. B* **94**, 214416 (2016).
- [60] Y. Teng, Y. Zhang, R. Samajdar, M. S. Scheurer, and S. Sachdev, Unquantized thermal hall effect in quantum spin liquids with spinon fermi surfaces, *Phys. Rev. Res.* **2**, 033283 (2020).
- [61] S. Zhang, S. Lee, E. Brosha, Q. Huang, H. Zhou, V. S. Zapf, and M. Lee, Out-of-plane magnetic phase diagram of kitaev quantum spin liquid candidate  $\text{na}_2\text{co}_2\text{teo}_6$ , arXiv preprint arXiv:2405.13935 (2024).
- [62] B.-B. Chen, Y.-J. Liu, Z. Chen, and W. Li, Series-expansion thermal tensor network approach for quantum lattice models, *Phys. Rev. B* **95**, 161104(R) (2017).
- [63] B.-B. Chen, L. Chen, Z. Chen, W. Li, and A. Weichselbaum, Exponential thermal tensor network approach for quantum lattice models, *Phys. Rev. X* **8**, 031082 (2018).
- [64] H. Li, B.-B. Chen, Z. Chen, J. von Delft, A. Weichselbaum, and W. Li, Thermal tensor renormalization group simulations of square-lattice quantum spin models, *Phys. Rev. B* **100**, 045110 (2019).



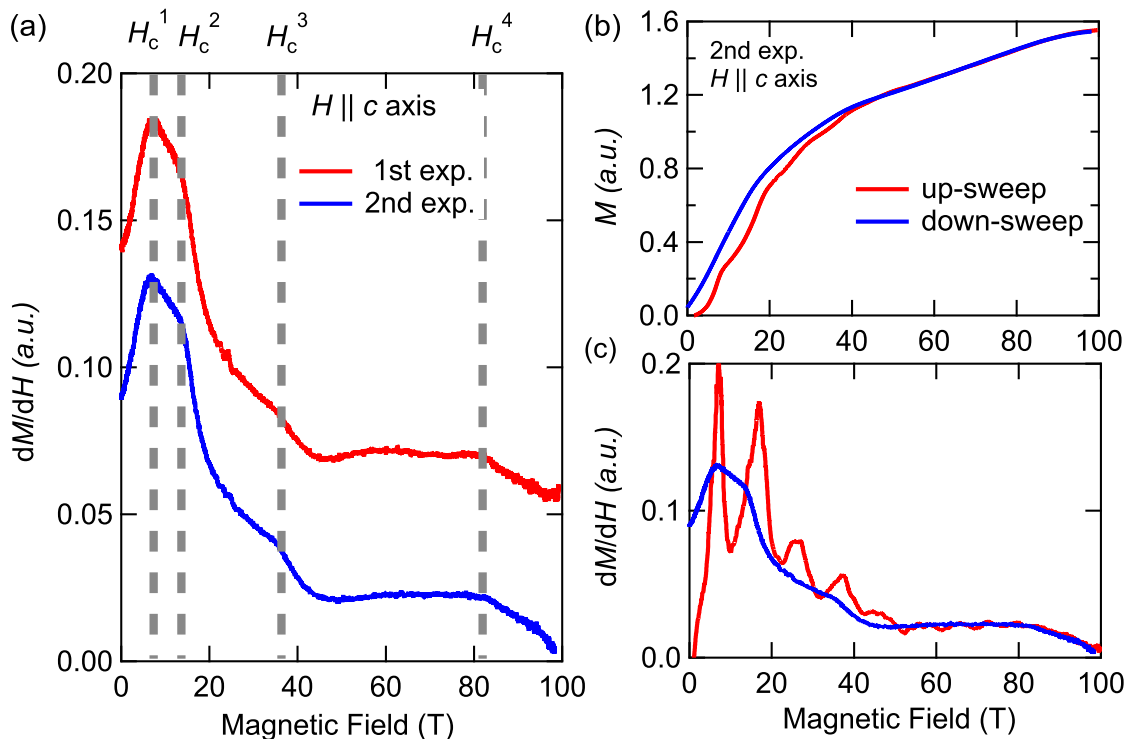


**Fig. S1. Reproducibility of magnetization measurement.** **a** The comparison between the first and second magnetization measurement for  $\theta \simeq 0^\circ$ ; **b** and **c** the comparison between up- and down-sweep data in the second magnetization measurement for  $\theta \simeq 0^\circ$ .

## Supplementary Materials

### A. Experimental details of Magnetization Measurement and Its Reproducibility

**Magnetization data.** To confirm the high field phase transition  $H_c^4$  for  $H \parallel c$  is not caused from the artificial effect, we present the magnetization results of two independent experiments, as shown in Fig. S1(a). The field values of phase transitions  $H_c^{1-4}$  show good agreement in these two independent experiments. We also show the good agreement between the up-sweep and down-sweep data in Fig. S1(b) and (c) for the second measurement. In the up-sweep result, the initial noise (from 0 to 50 T) prohibit the observation of small anomalies, such as  $H_c^3$ . Therefore, we only present the down-sweep magnetization data in the maintext.

### B. Determination of the Effective Model for $\text{Na}_2\text{Co}_2\text{TeO}_6$

**Results computed based on previous models.** In Fig. S2, through density matrix renormalization group (DMRG) method, we computed the magnetization curves with fields applied along  $\mathbf{a}^*$  and  $\mathbf{c}$ -axis for several spin models previously proposed for  $\text{Na}_2\text{Co}_2\text{TeO}_6$  [28, 32, 35, 37, 57]. The calculations are performed on the Y-type cylinder (YC)  $W \times L \times 2$  lattices with width  $W = 8$  and length  $L = 12$ , with bond dimension  $D = 256$  and truncation error less than  $10^{-5}$ . By converting to experimental units based on their reported energy scales [28, 32, 35, 37, 57], we observed discrepancies of transition fields between these simulated results and our measured curves, e.g., for the out-of-plane field along  $\mathbf{c}$  direction, neither of the computed results exhibits features indicative of two phase transitions at around 35 T and 82 T (see Fig. S2a-c,e-h). Consequently, we surmise that these models are not well-equipped to explain our experimental observations that presented in the main text.

**The effective Hamiltonian for  $\text{Na}_2\text{Co}_2\text{TeO}_6$ .** Drawing upon our previous experience in determining the Hamiltonian for  $\alpha\text{-RuCl}_3$  [55], we have refined it to propose the following parameters based on the  $K\text{-}J\text{-}\Gamma\text{-}\Gamma'$  honeycomb

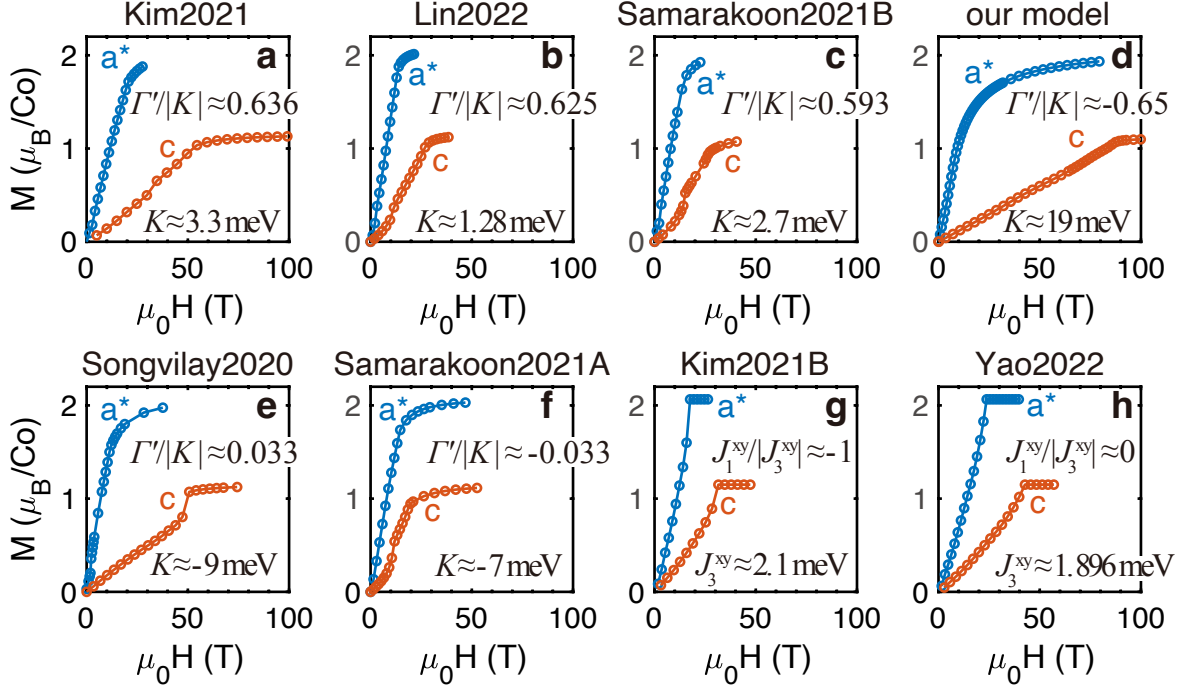


**Fig. S2. Magnetization curves of various proposed models for  $\text{Na}_2\text{Co}_2\text{TeO}_6$  by employing the DMRG method.** **a-c** In-plane and out-of-plane results with parameters from “Kim2021” [28], “Lin2022” [57], and “Samarakoon2021B” [37] with  $K > 0$ . **d** The calculated results by our model proposed in this work. **e,f** Magnetizations with parameters from “Songvilay2020” [35] and “Samarakoon2021A” [37] with  $K < 0$ . **g,h** Calculated curves by XXZ  $J_1$ - $J_3$  models proposed in “Kim2021B” [28] and “Yao2022” [32]. The energy scale (meV) and the ratio between typical  $\Gamma'$  and  $K$  interactions are indicated in each panel.

model:

$$H = \sum_{\langle i,j \rangle_\gamma} [K S_i^\gamma S_j^\gamma + J \mathbf{S}_i \cdot \mathbf{S}_j + \Gamma(S_i^\alpha S_j^\beta + S_i^\beta S_j^\alpha) + \Gamma'(S_i^\gamma S_j^\alpha + S_i^\alpha S_j^\beta + S_i^\beta S_j^\gamma + S_i^\gamma S_j^\gamma)]. \quad (\text{S1})$$

Here,  $\mathbf{S}_i = \{S_i^x, S_i^y, S_i^z\}$  represents the set of pseudo spin-1/2 operators acting at the  $i$  site. The parameter  $K = 19$  meV denotes the antiferromagnetic Kitaev interaction and is set as the energy scale;  $J = -0.9035K$  stands for the nearest-neighbor isotropic Heisenberg term;  $\Gamma = -0.65K$  and  $\Gamma' = 0.3597K$  are the non-Heisenberg exchange couplings. The notation  $\langle i, j \rangle_\gamma$  signifies a nearest-neighbor pair connected by a  $\gamma$ -type bond, where  $\{\alpha, \beta, \gamma\}$  refers to a cyclic permutation of  $\{x, y, z\}$ .

**The magnetization process under tilted field angles.** Based on the above parameters, we can calculate the magnetization results under various tilted fields applied within the  $\mathbf{a}^*\mathbf{c}$ -plane as shown in Fig. S3a-f (also in Fig. S2d). The angle  $\theta$  with respect to  $\mathbf{c}$ -axis indicating the direction of field and is represented by  $\cos(\theta)[\sqrt{\frac{1}{3}} - \sqrt{\frac{1-\cos^2(\theta)}{2\cos^2(\theta)}}]$ ,  $\sqrt{\frac{1}{3}}$ ,  $\sqrt{\frac{1}{3}} + \sqrt{\frac{1-\cos^2(\theta)}{2\cos^2(\theta)}}$  in the spin space  $(S^x, S^y, S^z)$ . We find the curves and their derivatives for different  $\theta$  exhibit trends that are in agreement with experimental measurements and are largely consistent in a qualitative sense. For example, under perpendicular magnetic fields ( $\mu_0 H \parallel \mathbf{c}$ ,  $\theta = 0^\circ$ , see Fig. S3f), the dM/dH curve exhibits two peaks corresponding to the transition fields  $\mu_0 H_3 \simeq 33$  T and  $\mu_0 H_4 \simeq 86$  T measured experimentally; while for the in-plane field case ( $\mu_0 H \parallel \mathbf{a}^*$ ,  $\theta = 90^\circ$ , see Fig. S3a), the phase transition occurs only at about 6 T. The calculations are performed on  $\text{YC}4 \times 6 \times 2$  lattices, with kept bond dimension  $D = 512$ .

**Intermediate disorder phase.** The two transition fields at  $H_3$  and  $H_4$  under the perpendicular magnetic field (see Fig. S3f) indicates the presence of an intermediate phase. In the bottom panels of Fig. S3, we have computed the static spin-structure factors with zero field (Fig. S3g) and within the low-field phase ( $\mu_0 H \simeq 25$  T, Fig. S3h), intermediate-field phase ( $\mu_0 H \simeq 68$  T, Fig. S3i), and saturated field conditions ( $\mu_0 H \simeq 103$  T, Fig. S3j), subtracting the influence of the magnetic field background. At low magnetic fields, we find that there is a notable intensity peak

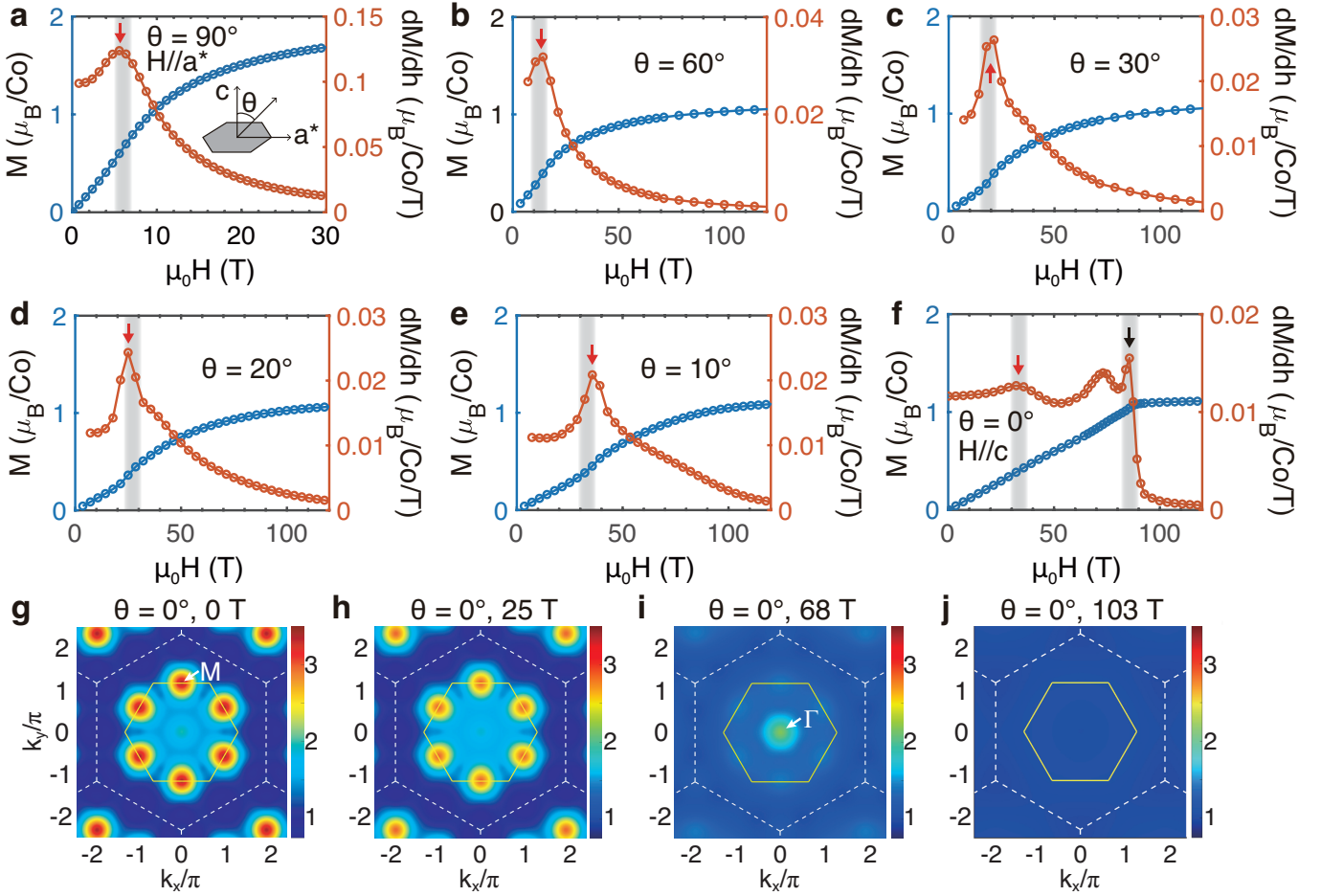


**Fig. S3.** Magnetization process under tilted fields and the spin-structure factors. **a-f** Magnetization curves and their derivatives under different  $\theta$  angles within the  $\mathbf{a}^*\mathbf{c}$ -plane, where the shaded regions indicate the field strength of phase transitions as measured experimentally, and arrows denote the transition fields obtained from DMRG calculations based on our  $K$ - $J$ - $\Gamma$ - $\Gamma'$  model. **g-j** Contour plots of static spin-structure factors at various magnitudes of the  $\mathbf{c}$ -axis magnetic field, i.e., **g** 0 T, **h** 25 T, **i** 68 T and **j** 103 T.

observed at the M-point [c.f., Fig. S3g,h]. These observations are consistent with the low-field results in neutron experiments [32, 57, 59]. In the intermediate-field regime, the antiferromagnetic order at M-point is suppressed, and the static spin-structure factor does not manifest any characteristic peaks but exhibits some brightness at the  $\Gamma$  point [c.f., Fig. S3i]. Such results resemble those found in  $\alpha$ - $\text{RuCl}_3$  [55], supporting the hypothesis that the intermediate phase is a disordered state (potentially a quantum spin liquid with either no gap or a very small gap [56]). Upon subtracting the magnetic field background in the high-field regime, no features are observed [Fig. S3j], suggesting that the phase above the transition field  $H_4$  corresponds to a trivial paramagnetic phase.

### C. The calculated magnetocaloric effect based on the effective spin model

**Calculated results of the magnetocaloric effect curves.** In Fig. S4, we show the magnetocaloric effect (MCE) results with isentropes originating from a range of low temperatures. The finite-temperature calculations are performed by exponential tensor renormalization group (XTRG) method [62–64] on the  $\text{YCW} \times L \times 2$  lattices, with width  $W = 4$  and length  $L = 6$ , and bond dimension  $D = 200$ . The magnetic field is applied along  $\mathbf{c}$ -axis.

Within the low-field regime, these curves exhibit a persistent increase as the magnetic field strength is enhanced. Notably, a pronounced enhancement is observed around 35 T, consistent with the proposed transition field  $H_c^3$ . Given that the low-field transitions,  $H_c^1$  and  $H_c^2$ , are associated with the reorganization of antiferromagnetic order [33, 34, 53], and are likely influenced by three-dimensional interactions, they fall beyond the scope of our calculations based on

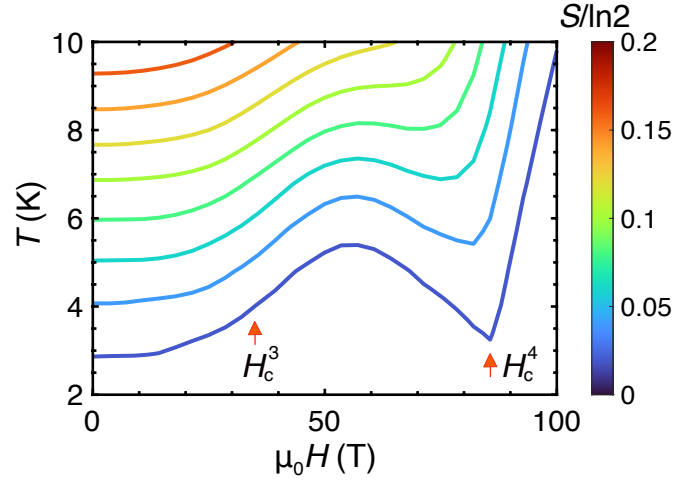


**Fig. S4. Magnetocaloric effect calculated by the XTRG method.** The field is applied along  $c$ -axis ( $\theta = 0^\circ$ ), and the color coding indicate the values of thermal entropy  $S/\ln 2$ . Two transition fields  $H_c^3$  and  $H_c^4$  determined from the DMRG results are also indicated by the red arrows.

the effective two-dimensional spin models. In the high-field regime, an intriguing feature is observed: a dip in the isentropes, which becomes evident at approximately 86 T, near the transition field  $H_c^4$ . Such curves are also in excellent agreement with the ground-state DMRG data. Therefore, we note that the calculated MCE data not only corroborate the experimental evidence but also suggest further detection for the intermediate-field quantum disordered phase. If experiments could be conducted at higher magnetic fields, MCE studies would be crucial in exploring and confirming the existence of this phase.